Parametric Study of Ultrasuperhydrophobic Nanotextured Microstructured Surface Topographies Produced by Picosecond Laser Micromachining on H13 Tool Steel

Evgueni Bordatchev[*1,2] and Honghe Wu[2,1]

[1]*Automotive and Surface Transportation Research Center,*
National Research Council of Canada, London, Ontario, Canada
[2]*Department of Mechanical and Materials Engineering*
Western University, London, Ontario, Canada
[*]*Corresponding author's email: hwu445@uwo.ca*

Hierarchical nano/microscale surfaces offer properties that are of high interest to industry, as they can enable value-added functionalities such as controlled frictional, optical, aerodynamic, hydrodynamic, and other phenomena. Advanced laser-based structuring/texturing technologies, such as direct laser writing, laser-induced periodic structuring, and direct laser interference patterning, are most prominent for high-speed, large-area, and cost-effective fabrications of micro/nano grooves, riblets, dimples, pillars, pyramids, and their geometric combinations. The focus of this study is to explore how surface topography components are responsible for producing hydrophobic, superhydrophobic, and ultrasuperhydrophobic (contact angles 160°…175°) surfaces by single-step picosecond laser micromachining. Four functional surfaces, including microstructured square pyramids with side lengths of 10, 20, 30, 40 μm and nanotextured riblets with feature sizes of <1 μm, were machined on H13 tool steel, and the relationship between topographic characteristics and hydrophobic performance were studied. The results demonstrate that all features are synergistically responsible for the hydrophobic performance within a range of contact angles between 140° and 175°. The most critical role in obtaining superhydrophobic and ultrasuperhydrophobic performance was played by laser-induced nanoriblets on top of periodical microstructures. When nanoriblets were removed by flattening the top surfaces, wettability performance dropped from 175° to 139° contact angles. These results lay a scientific and engineering basis for hierarchical surface formation by laser processing and identify statistical metrics affecting surface wettability for the future development of fully controlled and optimized hydrophobic–hydrophilic surfaces.
DOI: 10.2961/jlmn.2023.02.2006
Keywords: surface, nanotexture, microstructure, picosecond laser micromachining, hydrophobicity

1. Introduction

Specific designs of surface topographies, e.g., especially bioinspired designs [1] such as shark skin, fish scales, lotus leaves, moth eyes and many others, can enable value-adding functionalities such as controlling frictional [2], optical [3], aerodynamic [4], hydrodynamic [5], and other well-known surface properties. Well-known geometric micro/nano features such as grooves, riblets, dimples, pillars, pyramids, and others can be produced at micro- and nanometer scales by a significant variety of micromachining processes [6, 7]. However, the laser-based material processing of functional surfaces [8] is likely the most universal surface engineering technology, spreading from material subtractive processes such as laser micromachining [9] to material additive technologies [10].

Currently, high-precision laser micromachining is probably the best and most versatile technology for the cost-effective high-speed production of functional surfaces, especially with superhydrophobic and superhydrophilic performance, in different materials. Three variations of laser ablation-based micromachining technology are commonly used for producing surface topographies with wettability-controlled phenomena. They include a) the direct laser writing (DLW) of microscale surface structures by creating grooves and dimples [11]; b) the formation of spatially random laser-induced periodic structures [12] as micro/nanoscale pillars; and c) the patterning by direct laser interference [13] of spatially controlled micro/nanoscale grooves.

Significant improvements in the superhydrophobicity (with a contact angle (CA) of >150°) of metallic and non-metallic surfaces have been enabled by producing combined hierarchical periodic surface structures as a geometric combination of nanotexture and microtopography [14]. Such complex surface topographies are produced by combining at least two laser microfabrication technologies—direct writing for creating microstructures and either laser-induced periodic surface structuring (LIPSS) [15] or direct laser interference patterning (DLIP) [16]—to achieve a CA of 158° on stainless steel alloy AISI304 and a CA of 163° on pure aluminum, respectively.

This study continues to advance the development of superhydrophobic and superhydrophilic surfaces [17] by a DLW process. The combination of micropillars, microgrooves, nanoriblets, and deep blind micropits were explored to determine which are responsible for producing

ultrasuperhydrophobic (contact angle between 160° and 175°) surfaces by single-step picosecond laser micromachining technology combined with DLW and LIPSS processes. Detailed attention was placed on the contribution of nanotextures (N-T) (e.g., nanoriblets) produced by the LIPSS over the top surface of microstructures (M-S) (e.g., micropillars) produced by DLW in ultrasuperhydrophobic functional performance.
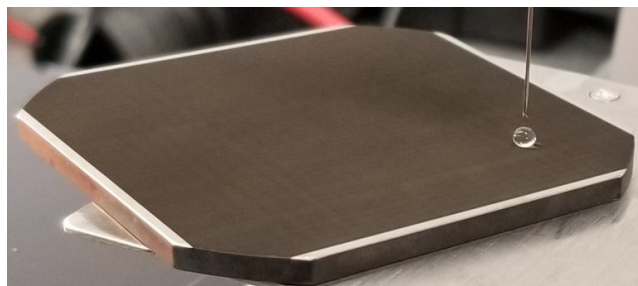
2. Laser micro/nanomachining system

Figure 1 illustrates the modular multifunctional Microgantry Nano5x micromachining system from Kugler GmbH, Salem, Germany, used for N-T/M-S laser micro/nanoprocessing. The micromachining system includes three linear axes (X, Y, and Z) and two rotary axes (A and C). The motion stages are suspended on air bearings and have a positional resolution of 10 nm with a static positioning accuracy of ±100 nm, a dynamic positioning accuracy of ±1.0 μm, and a micromachining accuracy of ±1.0 μm. All three linear axes have a straightness within ±800 nm per 100 mm of travel. The micromachining system was integrated with a DPSS MOPA near-Gaussian laser with a wavelength of 1064 nm, a pulse width of 10.5 ps, a repetition rate of up to 8.2 MHz, and a maximum power of 12 W. A volumetric flow of argon along the laser beam path was maintained toward the vicinity of the laser material interaction zone to induce a neutral processing zone. In addition, the system performs workpiece alignment and postmachining geometry verification by means of a Renishaw touch probe characterized by a measurement accuracy of ±500 nm and a measurement repeatability (2σ) of 100 nm.
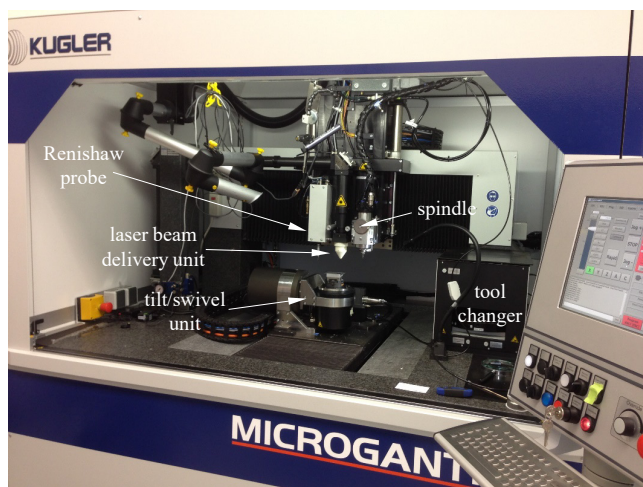
Fig. 1 Experimental setup: High-precision, multiprocess multiaxis micromachining system.

Flat samples with dimensions of 60 mm ×60 mm ×3 mm were made from H13 tool steel as a most common material for tool and die industry in Canada. Top surface of the samples was flattened by grinding obtaining initial areal surface roughness S_a of 520 nm. Also, samples were cleaned by placing into an ultrasonic bath with isopropanol for 20 min before laser processing. Four designs were studied having square tapering pyramids with a side length of 10, 20, 30, 40 μm and textured by nanoriblets with a period of ~1 μm. Figure 2 shows a laser micro/nanomachined sample with N-T/M-S surface topography produced with a laser fluence of 111.4 mJ/cm² and a scanning speed of

800 mm/min, with 1 MHz pulse frequency. To ensure the creation of isotropic properties, the samples were processed in a crosshatch pattern in alternating X and Y directions with a total of two passes. Following laser processing, the samples were cleaned again of accumulated laser ablation products, leaving only the permanent micro and nano features. In addition, samples were kept in a temperature-controlled chamber at 50°C to prevent environmental oxidation and corrosion.

Fig. 2 Laser micro/nanomachined sample with N-T/M-S surface.

3. Surface topography analysis methodology

Several research studies have already demonstrated significant improvement of the hydrophobic performance of micro/nano combined periodically structured hierarchical surfaces [14-17]. Typically, as shown in Figure 3, such surfaces will be formed by a complex spatial combination of micro- and nanogeometric features, such as a) microgrooves forming rectangular micropillars by DLW, b) deep blind micropits formed by intercepted microgrooves during DLW, and c) nanoriblets formed by LIPSS and located on the grooved walls and top surfaces of micropillars. It is obvious that all these geometric features synergetically contribute to the hydrophobic functional performance, and classic Young, Wenzel, and Cassie equations [18] may not be applicable for modeling the wettability of such complex surface topographies.

This research attempts to extract and analyze the combined N-T/M-S and separated N-T and M-S surface topographies on the hydrophobic behavior of a functional surface. It appears that this goal can only be achieved on typical rectangularly microstructured geometries with nanotextured topography on the top surface. Therefore, an experimental study was proposed for two functional surfaces: a combined N-T/M-S geometry (as fabricated) and its modification as an M-S geometry, where the top surface was flattened by fine abrasive polishing to remove the nanotextured top surface, as shown in Figure 4. In this case, the flattened sample includes only a) microgrooves forming rectangular micropillars by DLW, b) deep blind micropits formed by intercepted microgrooves, and c) top-flattened square tapering pyramids.

Laser micromachined N-T/M-S surface topographies with an area of 0.55 mm×0.55 mm were measured with a WYKO NT1100 optical profilometer with lateral and vertical resolutions of 93.7 nm and 0.1 nm, respectively. An example of a measured N-T/M-S surface topography is shown in Figure 5. Such high lateral resolution was needed to capture the surface topography of the nanoriblets. For each measured surface topography, a 12×12 pyramid matrix was extracted for further analysis of the two most criti-

cal characteristics: areal parameters of the surface geometry in accordance with the ISO 25178 standard and a power spectral density (PSD) representing a frequency distribution of the topography micro/nanofeatures. The following specific areal parameters were calculated, analyzed, and compared for micromachined and flattened topographies: areal root mean square (RMS) roughness (S_q), percentage of additional surface area (S_{dr}), and summit density (S_{ds}) within frequency ranges of 10…500 mm^{-1} and 500…5000 mm^{-1}. N-T and M-S are both critical to the hydrophobic performance, which is why S_{ds} was analyzed at high and low frequency ranges.
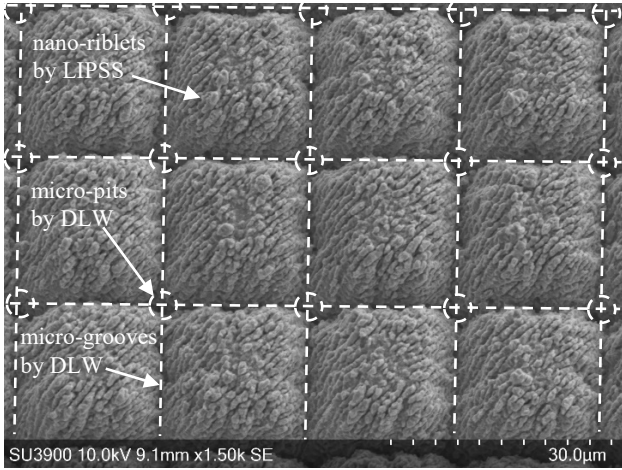
Fig. 3 Typical SEM image of the N-T/M-S surface topography.
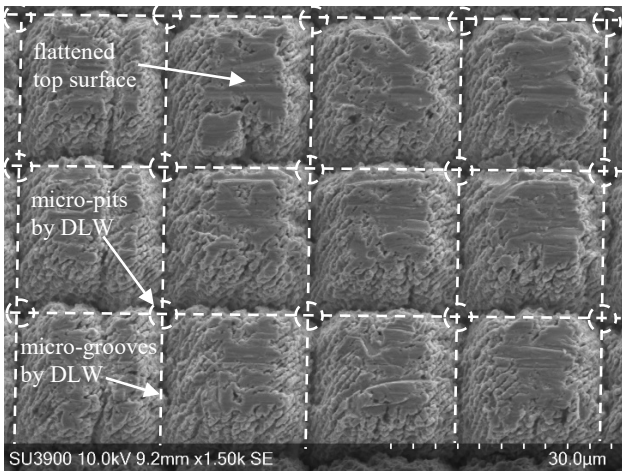
Fig. 4 Typical SEM image of flattened M-S surface topography.

4. Parametric analysis of surface topographies and their ultrasuperhydrophobic performance

Four large-size functional surfaces were produced with different side lengths of 10, 20, 30, 40 µm of square tapering pyramids. SEM images of the laser processed surfaces are presented in Figure 6, and their flattened copies are shown in Figure 7. It is necessary to note that the surfaces with 10 µm and 20 µm side pyramids are fully covered (100%) by nanoriblets due to the LIPSS process with a total width around a microgroove of ~20 µm. Concurrently, the surfaces with 30 µm and 40 µm side pyramids are only partially covered by the LIPSS-produced nanoriblets at 11.1% and 44.4%, respectively.
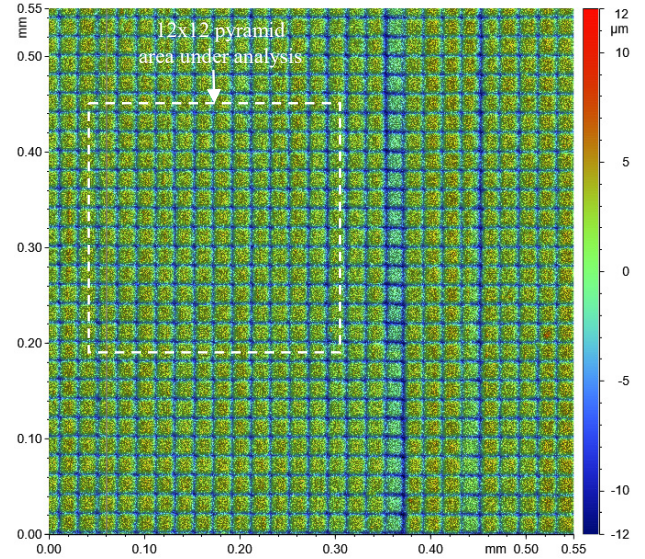

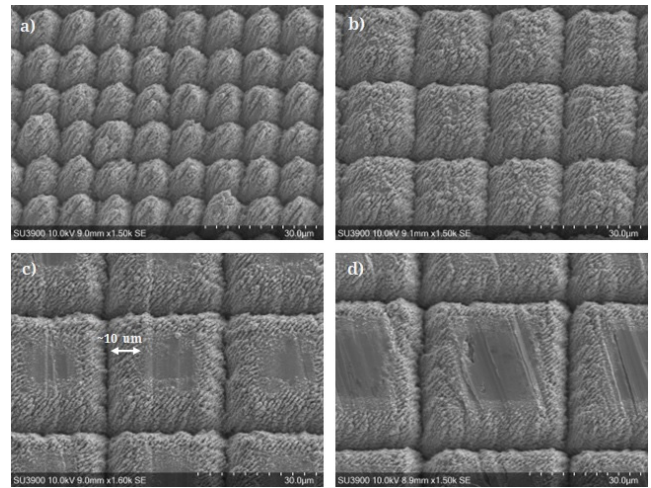**Fig. 5** Example of measured N-T/M-S surface topography.

Fig. 6 SEM images of nanotextured microstructured surfaces: a) 10 µm, b) 20 µm, c) 30 µm, and d) 40 µm.
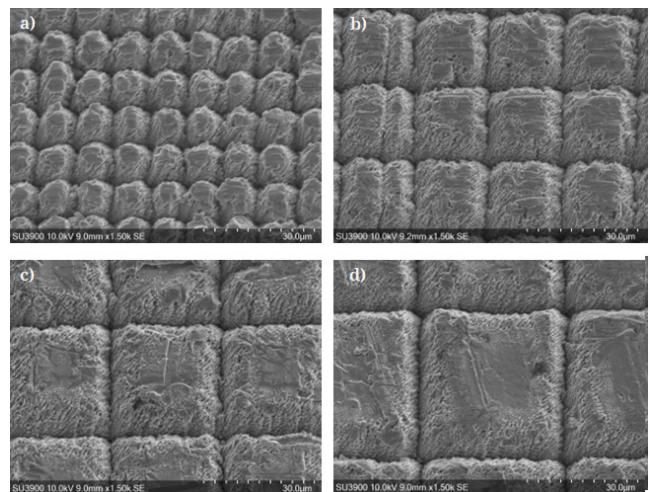
Fig. 7 SEM images of flattened nanotextured microstructured surfaces: a) 10 µm, b) 20 µm, c) 30 µm, and d) 40 µm.

The ratio between the area covered by nanoriblets and the total area of the pyramid plays an important role in forming hydrophobic functionality. Therefore, this ratio

was increased by flattening the pyramids, as shown in Figure 7. It can be assumed that water drops will be sitting on three different dimensional geometrical features: nanoriblets with a width <1 μm, as shown in Figure 8, flat rectangular micropillars, and microgrooves.

More detailed information about the geometry of laser-processed N-T/M-S functional surfaces can be obtained from their lateral cross-sections depicted in Figure 9. It can be observed that 10, 20, 30, 40 μm periodic structures were produced with an accuracy of ±1 μm, an average microgroove depth of 9–10 μm, and an average micropit depth of ~15 μm. For rectangular micropillars with a side length of 10 μm, a width-to-height aspect ratio of 1:1.5 was achieved, which is outstanding for ultrashort pulse laser micromachining of high aspect ratio functional structures and textures [19].
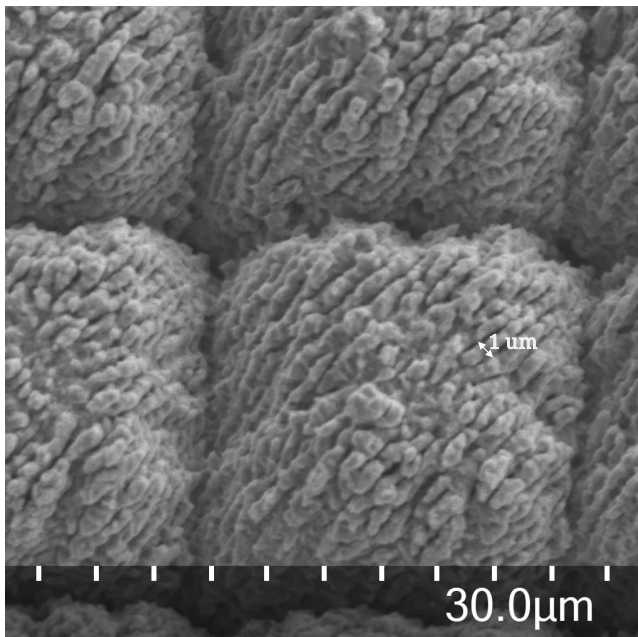

Fig. 8 SEM image of typical laser-induced periodic structures.

To fulfill the scope of this study, the top surface of the as-fabricated samples was flattened to remove spatial high-frequency LIPSS components from the top surface, as depicted in Figure 7. It is obvious that the N-T/M-S surface is a geometrical superposition of the M-S form geometry with a period of the pyramid side length as a low spatial frequency component and nanotexture as a high spatial frequency component. A comparison of the PSD functions of the as-machined and flattened N-T/M-S topographies is shown in Figure 10 for the 20 μm functional surface. The main common feature of the two PSD functions is similar amplitudes of the 1st, (50 1/mm = 1/20 1/μm), 2nd (100 1/mm), 3rd (200 1/mm), and 4th (400 1/mm) harmonics. However, all other frequency components are less than ~15%, which is also supported by decreasing a total 2D RMS value of 39.08 nm for the as-machined surface to 23.2 nm for the flattened surface.

Such significant changes in surface topography characteristics are also supported by height distribution histograms depicted in Figure 11. For a flattened surface, the distribution of surface heights is much shorter, the number of amplitudes within the ±1 μm range corresponding to the N-T LIPSS features is smaller, and the variation in surface

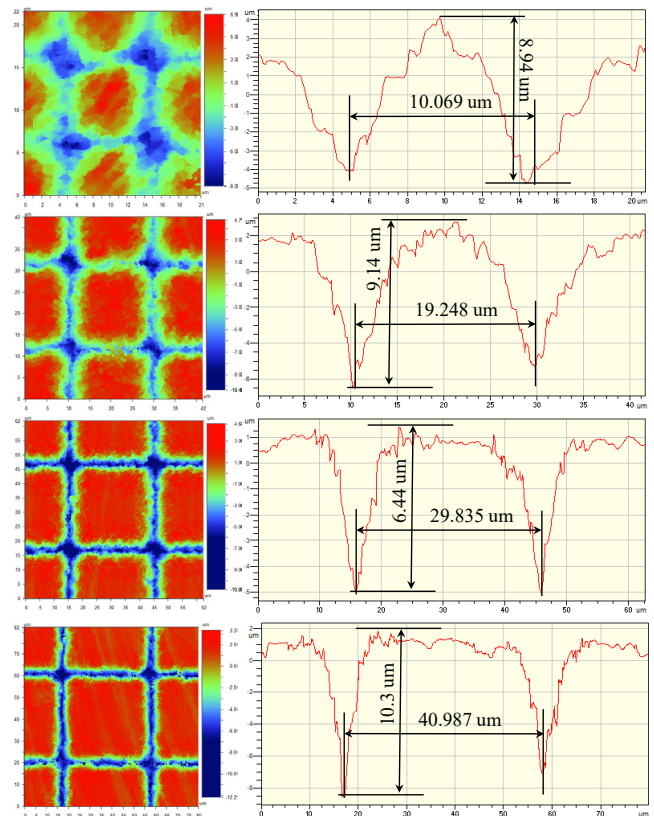amplitudes is dominated more by microgrooves than nanoriblets.

Fig. 9 Lateral cross-sections of N-T/M-S functional surfaces.

The parametric study of N-T/M-S surfaces presented above lays a foundation and comprehensive understanding of how micro- and nanocomponents of such complex topographies contribute to hydrophobic functional performance. For this purpose, a commercial system (Kruss DSA30E Drop Shape Analyzer) was used to measure contact angles seven times for each surface and in different locations. All measurement results and comparison of contact angles for as-fabricated and flattened NT-MS surfaces are depicted in Figure 12. Contact angle mean values for 10, 20, 30, 40 μm periodical structure designs and their standard deviations (STD) are presented in Table 1. These CA numbers were achieved on a 2nd day and were measured every day during 3 weeks. The samples still exhibit ultrasuperhydrophobic performance a year thereafter.

Table 1 Mean and STD values of measured contact angles

Period	Mean value		STD value	
	as-machined	flattened	as-machined	flattened
10 μm	171.9°	139.1°	2.2°	1.1°
20 μm	160.2°	141.1°	2.6°	1.9°
30 μm	150.0°	142.6°	2.5°	1.6°
40 μm	144.9°	145.1°	1.2°	2.5°

Superhydrophobic phenomena (CA > 150°) were achieved for three designs with 10, 20, 30 μm periodical structures. By comparing contact angles achieved on as-machined and flattened samples (see Table 1 and Figure 12), it becomes evident that the presence of the LIPSS

nanoriblets on top of the microsquare structures is the main contributor in achieving superhydrophobicity with a contact angle >160°. This is achieved by the Cassie wetting condition when a water droplet is supported by a combination of nanoriblets, air pockets between them, and air pockets formed by microgrooves and micropits. It is also remarkable that ultrasuperhydrophobic performance with a CA >170° was achieved on 10 µm periodic structures fully covered with nanoriblets, as shown in Figure 13.

Fig. 12 Comparison of contact angles for as-fabricated and flattened NT-MS surfaces.
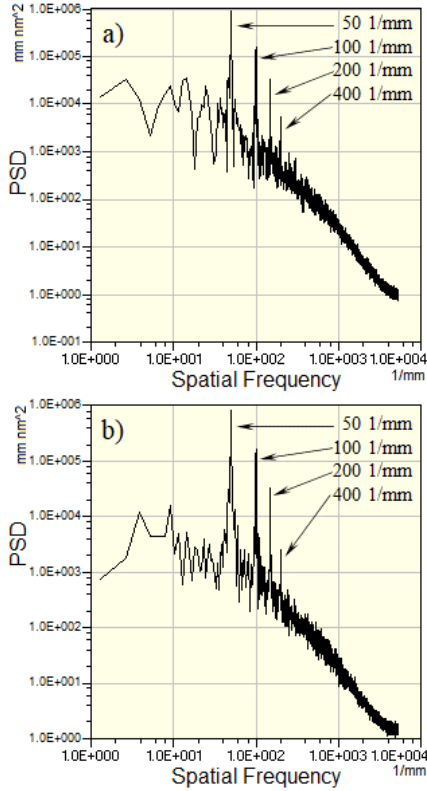

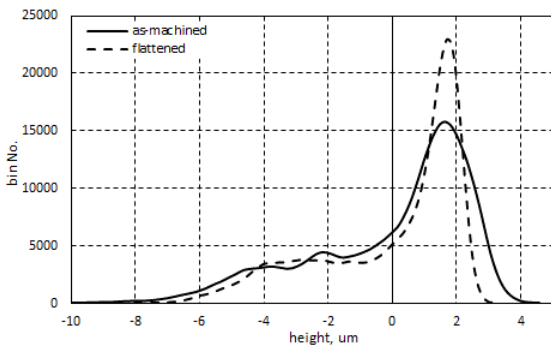**Fig. 10** PSD functions: a) as-machined and b) flattened surfaces.

Fig. 11 Histograms of as-machined and flattened surfaces.

Flattening of the top surfaces of the microsquare structures significantly reduces the hydrophobic performance, e.g., by 19.1% for 10 µm structures. This is because the wetting state changes from the Cassie to Wenzel condition on the top surface and retains the Cassie condition on the microgrooves and micropits.

This parametric study shows that the squared M-S is fully responsible for the base contact angles when wettability is defined by the microscale form and geometry. Flattening by removing nanoriblets on top of the squared structures changes the contact geometry and area. These
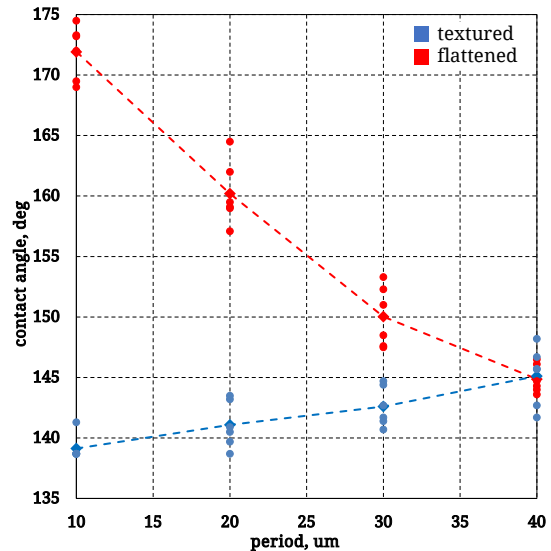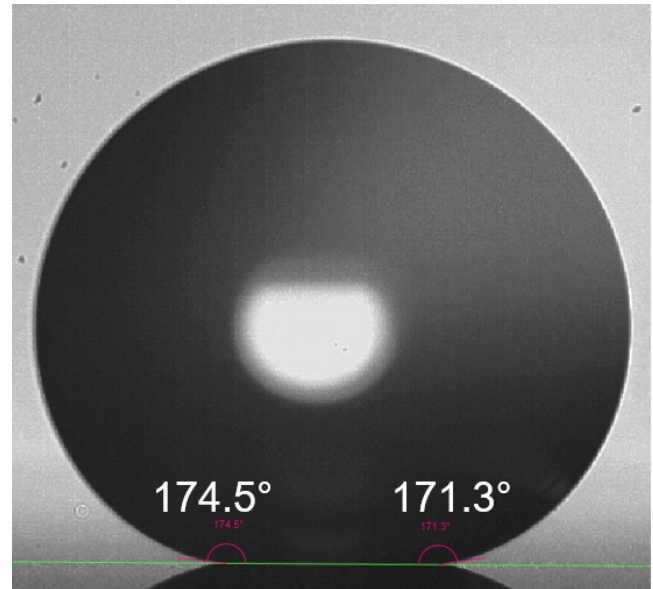

Fig. 13 Example of ultrasuperhydrophobic contact angles.

changes can be fully characterized by calculating several topography characteristics, such as areal RMS roughness (S_q), percentage of additional surface area (S_{dr}), and summit density (S_{ds}), within waviness and roughness spatial frequency ranges of 10–500 mm^{-1} and 500–5000 mm^{-1} in accordance with the ISO 25178 standard. In general, the S_q value estimates the overall variability of the entire surface topography. As expected, the effect of flattening the top surface corresponded to a reduction in the S_q value. For an example of 20 µm structures, reductions of S_q for total 12×12 structures and its spatial frequency components as waviness (representing microstructures) and roughness (representing nanotextures) by 10.5%, 10.3%, and 3.3% were calculated and demonstrated in Figure 14. It is necessary to note that S_q as an overall parameter may not reliably represent an impact of the surface topography on the surface wettability. Therefore, more mathematically complex characteristics such as S_{dr} and S_{ds} but with more evident physical and engineering meanings with respect to the surface wettability were also analyzed further.

The value of S_D, called the developed interfacial area ratio, expresses the percentage of additional surface area contributed by the texture/structure compared to an ideal plane area (flat) of the measurement region. From the engineering perspective, topography with as-machined high aspect ratio structures contributes to S_{dr} more than flattened topography over the entire surface and in waviness and roughness components, as shown in Figure 15. From the wettability perspective, higher values of S_{dr} will enhance the hydrophobic performance, which is confirmed by Figure 12 for 20 µm structure topographies.
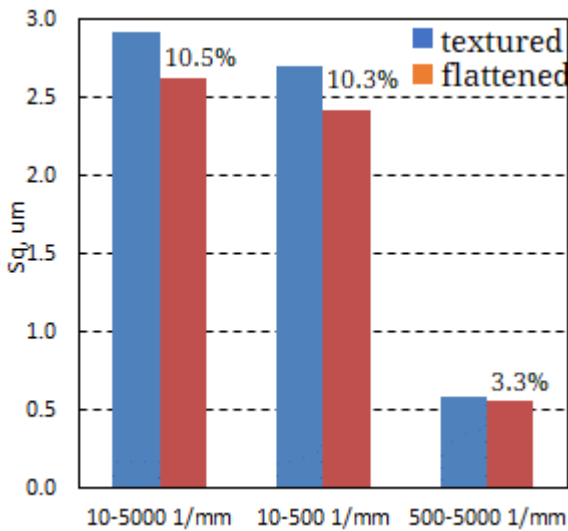

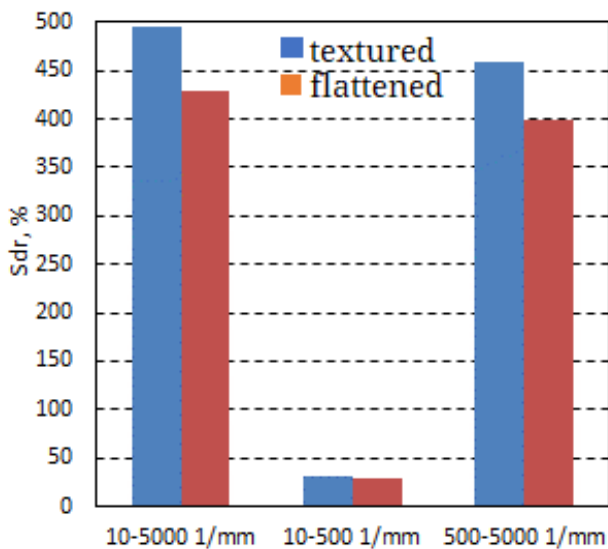**Fig. 14** Comparison of S_q and its spatial frequency components.

Fig. 15 Comparison of S_{dr} and its spatial frequency components.

However, wettability is affected not only by the contact interface area [18] but also by a number of contact interface points. It is logical that hydrophobicity will be increased with a higher density of contact points per area that can be reliably estimated by an S_{ds} parameter. The value of S_{Ds} estimates the summit (contact point) density per unit area of the surface. In this study, S_{ds} values were calculated for

total as-machined and flattened 20 µm topographies in $1/mm^2$ units, including contributions from waviness and roughness components. Similar to the S_{dr} analysis results, the S_{ds} values are smaller for the flattened topography by 13.3%, 10.3%, and 13.31% for total topography, waviness, and roughness, respectively. This means that there is a smaller number of contact points (summits), and thus contact angles are significantly less for the flattened topographies (see Figure 16).
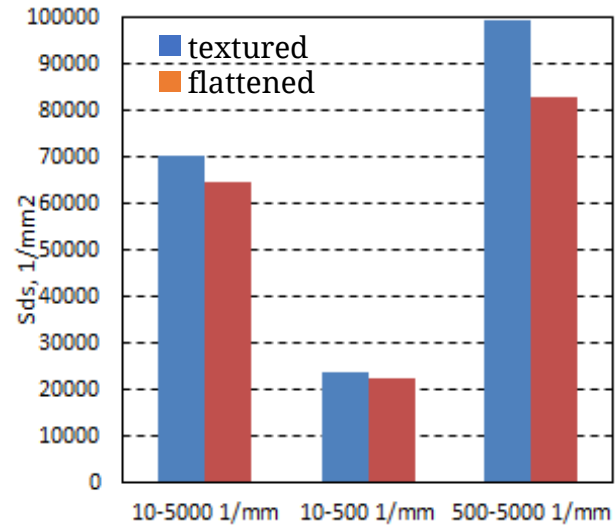

Fig. 16 Comparison of S_{ds} and its spatial frequency components.

5.   Summary and Conclusions

The work presented in this study outlines a parametric analysis of nanotextured microstructured surface topographies produced by picosecond laser micromachining and their relationships/correlations with surface wettability and hydrophobicity. A combined direct laser writing and laser-induced surface structuring process was exploited to fabricate N-T/M-S surfaces as a geometrical integration of micropillars, microgrooves, and deep blind micropits produced by DLW and nanoriblets generated by LIPPS. Four N-T/M-S surfaces with 10, 20, 30, 40 µm square tapering pyramids were attained, and their topography and hydrophobic performance were systematically analyzed. Detailed attention was placed on the contribution of nanoriblets on the top surface of the microstructures to the hydrophobic functional performance. In this regard, laser processed surfaces were evaluated by using scanning electron microscope (SEM) images and statistical characteristics and parameters of measured three-dimensional (3D) topographies, such as areal root mean square roughness, percentage of additional surface area, summit density, power spectral density, and amplitude distribution histogram.

The qualitative assessment facilitated the following conclusions to be drawn:

- Surface engineering by the one-step combined DLW and LIPSS process is efficiently capable of producing complex hierarchical nano/microtopographies with advanced functionalities, such as superhydrophobicity. This was demonstrated by fabricating microstructures as small as 10 µm with embedded <1 µm nanofeatures.
- The wettability performance of N-T/M-S surfaces linearly decreases from being remarkably ultrasuper-

hydrophobic (CA > 170°) on 10 μm structures to demonstrating superhydrophobic (CA = 150°…160°) performance on 20 μm and 30 μm structures and hydrophobicity with CA = 145° on 40 μm structures. Such wide-range precise control of the surface wettability opens new industrial applications of functional surfaces toward self-cleaning, biofouling prevention, and reconfigurable hydrodynamic and aerodynamic performance.

• Controllability of the hydrophobic performance was achieved by the ratio between the areas covered by the LIPSS nanoriblets and the top surface of the microsquare structures formed by the DLW ranging from fully covered by N–S microstructures. This was achieved for 10 μm periodic structures, as the width of the N–S area was also 10 μm.

The obtained results open new opportunities in developing laser fabrication and achieving novel and/or advanced functional performances of spatially distributed, functionally optimized, and fully controlled 3D surface topographies with respect to their interface with water, oil, air, molten materials, and other types of adjacent media.

References
[1] A. Malshe, K. Rajurkar, A. Samant, H.N. Hansen, S. Bapat, and W. Jiang: CIRP Annals – Manuf. Tech., 62, (2013) 607.
[2] G. Dumitru, V. Romano, H.P. Weber, H. Haefke, Y. Gerbig, and E. Pflüger: Appl. Phys. A, 70, (2000) 485.
[3] D. Hauschild: Laser Focus World, 11, (2017) 33.
[4] D. W. Bechert and W. Hage: Flow Phenomena in Nature, 2, (2006) 457.
[5] M. Ferrari and A. Benedetti: Adv. Colloid Interface Sci., 222, (2015) 291.
[6] S. Zhang, Y. Zhou, H. Zhang, Z. Xiong, and S. To: Int'l. J. of Mach. Tools and Manuf., 142, (2019) 16.
[7] E. Brinksmeier, B. Karpuschewski, J. Yan, L. Schönemann: CIRP Annals – Manuf. Tech., 69, (2020) 717.
[8] L.A. Dobrzański and A.D. Dobrzańska-Danikiewicz: Mater. Perf. and Charact., 8/6, (2019) 1091.
[9] F. Moglia, J. Pozo, and A. F. Lasagni: PhotonicsViews, 2, (2020) 20.
[10] F. Esteve, D. Olivier, Q. Hu, and M. Baumers: "Micro-Manufacturing Technologies and Their Applications" ed. by I. Fassi and D. Shipley, (Springer International Publishing, Switzerland, 2017) pp. 67-95.
[11] H. Shimada, S. Kato, T. Watanabe, and M. Yamaguchi: Lasers in Manuf. and Mat. Proc., 7, (2020) 496.
[12] C. Florian, S. V. Kirner, J. Krüger, and J. Bonse: J of Laser App., 32, (2020) #022063.
[13] L. Mulko, M. Soldera, and A.F. Lasagni: Nanophotonics, 11, (2022) 203.
[14] J. Noh, J.-H. Lee, S. Na, H. Lim, and D.-H. Jung: Jap. J of Appl. Phys., 49, (2010) #106502.
[15] M. Martínez-Calderon, A. Rodríguez, A. Dias-Ponte, M. C. Morant-Miñana, M. Gómez-Aranzadi, and S. M. Olaizola: Applied Surf. Sc., 374, (2016) 81.
[16] S. Milles, J. Dahms, M. Soldera, and A. F. Lasagni: Materials, 14, (2021), #184.
[17] P. Serles, S. K. Nikumb, and E. V. Bordatchev: J. of Laser Applications, 30, (2018) #032505.
[18] E. Y. Bormashenko: "Wetting of Real Surfaces," (Berlin, Boston: De Gruyter, 2019) p.178.
[19] T. Aizawa and T. Inohara: "Micromachining" ed. by Z. Stanimirović and I. Stanimirović, (Intechopen, 2019) p.172.